Biochemical and Biophysical Research Communications 747 (2025) 151281

Contents lists available at ScienceDirect

Biochemical and Biophysical Research Communications

journal homepage: www.elsevier.com/locate/ybbrc

Structural snapshots of the aldol condensation reaction of the enzyme *trans-o*-hydroxybenzylidenepyruvate hydratase-aldolase from *Pseudomonas fluorescens* N3

Silvia Ferrara [a,b], Bianca Braggiotti [a], Eloise Mastrangelo [a,b], Patrizia Di Gennaro [c], Giovanni Bertoni [b], Mario Milani [a,b,*]

[a] Biophysics Institute, CNR-IBF, Via Corti 12, I-20133, Milano, Italy
[b] Department of Bioscience, University of Milan, Via Celoria 26, I-20133, Milano, Italy
[c] Department of Department of Biotechnology and Biosciences, University of Milano-Bicocca Piazza Dell'Ateneo Nuovo, I-20126, Milano, Italy

ARTICLE INFO

Keywords:
Crystal structure
Aldolase
Intermediate state
Enzyme activity

ABSTRACT

Aldolases are crucial enzymes that catalyze the formation of carbon-carbon bonds in the context of the anabolic and catabolic pathways of various metabolites.

The bacterium *Pseudomonas fluorescens* N3 can use naphthalene as its sole carbon and energy source by using, among other enzymes, the *trans-o*-hydroxybenzylidenepyruvate (tHBP) hydratase-aldolase (HA), encoded by the *nahE* gene.

In this study, we present the crystallographic structures of *t*HBP-HA in three different functional states: the apo enzyme with a phosphate ion in the active site, and the Schiff base adduct bound either to pyruvate or to the substitute with '(R)-4-hydroxy-4-(2-hydroxyphenyl)-2-oxobutanoate'(intermediate state). Our structures elucidate some of the phases of the aldol condensation reaction, proposing the role of a conserved water molecule (W2) in the deprotonation of the catalytic lysine. Moreover, our crystallographic data suggest potential pathways for substrate and product diffusion to and from the protein's active site. These insights advance our understanding of the molecular mechanisms of the aldolase function and can also be used for the design and optimization of new enzymes engineered for the chemical synthesis of different C–C adducts.

1. Introduction

Aldolases catalyze the aldol reaction, a fundamental carbon-carbon bond-forming reaction in organic chemistry. Such reversible stereoselective addition of a donor compound (nucleophile) to an acceptor compound (electrophile) is involved in both the anabolism and the catabolism of metabolites in many biosynthetic pathways including carbohydrates, keto acids, and amino acids. Based on their enzymatic mechanism, aldolases are grouped into classes I and II. Class I aldolases activate the donor substrate by forming a Schiff base as an intermediate, thanks to a well-conserved lysine in the active site: in this way, the activated donor can be stereoselectively added to the acceptor aldehyde. Class II enzymes require a divalent metal ion as a cofactor for substrate binding and stabilization of intermediates, enabling the reaction to proceed through C–C bond formation or cleavage. Aldolases are also classified into four groups according to the donor type (among which the pyruvate-dependent aldolases). Members of class I show a conserved $(\beta/\alpha)_8$-barrel structure with tyrosine and lysine strictly conserved in the active site and a GXXGE motif associated with the binding of the pyruvyl carboxylate group.

The bacterium *Pseudomonas fluorescens* N3 can use naphthalene as the only carbon and energy source for its growth [1]. One of the steps of the naphthalene degradative pathway requires the activity of the aldolase encoded by the *nahE* gene. This enzyme, called *trans-o*-hydroxybenzylidenepyruvate (*t*HBP) hydratase-aldolase (HA), catalyzes the reversible conversion of *t*HBP in pyruvate and salicylaldehyde.

In a previous work, the aldol condensation activity of *t*HBP-HA was characterized using as substrates pyruvate and either salicylaldehyde or benzaldehyde [2], showing similar kinetic parameters for both compounds. Here, we report the crystallographic structure of *P. fluorescens* N3 *t*HBP-HA, which shares 95.8 % identity with NahE from *P. putida* (pdb-id 8do5 and 6dao). In particular, we describe the structure of three

* Corresponding author. Biophysics Institute, CNR-IBF, Via Corti 12, I-20133, Milano, Italy.
E-mail address: mario.milani@cnr.it (M. Milani).

https://doi.org/10.1016/j.bbrc.2024.151281
Received 12 December 2024; Accepted 31 December 2024
Available online 31 December 2024

different functional states of the protein: the free enzyme (with phosphate in the active site), the Schiff base pyruvate-bound state, and the intermediate-bound state. Our experimental results shed light on the phases of the aldol condensation reaction highlighting the role of a conserved water molecule (W2) as possible base for initial Lys deprotonation. Moreover, the crystallographic structures suggest possible diffusion pathways of the substrates/products to and from the protein active site.

2. Materials & methods

2.1. Gene sequence

The nucleotide sequence of *nahE* gene of *P. fluorescens* N3 is reported in the GenBank DataBase with accession number GU319975 (https://www.ncbi.nlm.nih.gov/genbank/).

2.2. Expression and purification of tHBP-HA

The expression and purification of recombinant N-terminal His-tagged aldolase were performed as already described [2]. Briefly, the pQE30 plasmid (Qiagen, Hilden, Germany), modified by inserting the coding sequence for aldolase as described (pQE30-ALD, [2]), was used to transform *E. coli* M15 (pREP4) (Qiagen). Bacteria were grown in M9 minimal medium at 37 °C with glucose (10 mM) as the carbon source, and in the presence of ampicillin and kanamycin (200 and 100 μg/ml, respectively). IPTG (1 mM) was added when the culture reached OD_{600} equal to 0.6 and the temperature was decreased to 30 °C. After 6 h, the pellet was collected and destroyed by sonication in ice (Soniprep 150-MSE); the lysate was cleared for 1 h at 24,000 g, applied to 2 ml of Co^{2+} TALON Metal Affinity Resin (Clontech, Euroclone, Milano, Italy), and eluted with a linear gradient of imidazole (from 50 to 250 mM). The imidazole was removed by dialysis against Na_2HPO_4/KH_2PO_4 50 mM, pH 7, overnight at 4 °C.

2.3. Crystallization and data collection

The purified protein (N-ter His-tag, Mw 38.3 kDa; calculated extinction coefficient 65,900 https://web.expasy.org/protparam/) concentrated to 6 mg/ml (in Na_2HPO_4/KH_2PO_4 50 mM, pH 7), was used to prepare crystallization trials with an Oryx8 nanodispenser robot (Douglas Instrument) using the sitting drop vapor-diffusion setup at 20 °C by mixing in each drop 0.2 μL of protein solution with 0.1 μL of precipitant solution. Crystals were obtained in different conditions of the Hampton crystal screen (HCS, Crystal Screen™; https://hamptonresearch.com). Crystals of the apo protein and of the intermediate-bound form were obtained in HCS condition 3, i.e. 0.4 M ammonium phosphate monobasic. To obtain the intermediate form, the protein (141 μM) was mixed with salicylaldehyde (2.5 mM) and pyruvate (2.5 mM) before crystallization, and also the cryoprotectant solution (25 % glycerol) was provided with salicylaldehyde and pyruvate (2.3 mM).

Crystals of the pyruvate bound form were obtained in HCS condition 35, i.e. 0.8 M sodium phosphate monobasic monohydrate, 0.8 M potassium phosphate monobasic, 0.1 M HEPES sodium pH 7.5, and soaked in the cryoprotectant solution (25 % glycerol) in the presence of pyruvate (10 mM) for 1 min before flash freezing in liquid nitrogen. X-ray diffraction data were collected at ESRF (Grenoble) beam lines ID14-1 and ID23-1 (Table 1).

2.4. Structure solution and analysis

The crystals of the apo protein and of the intermediate-bound forms were indexed and scaled using *imosflm* [3] and *scala* [4] (Table 1). The pyruvate-bound crystal was indexed and scaled using autoPROC Vonrhein et al., [5].

All structures were solved by molecular replacement (*MOLREP*, [6]) using as search model the crystal structure of NahE aldolase from *P. putida* (pdb-id 8do5; [7]) in its tetrameric assembly, finding two tetramers in the crystal asymmetric units (a.u.). In particular, pseudo-translation peaks were detected for all three crystals (21.8 % of the origin peak for the apo protein, 44.0 % for pyruvate-bound protein and 41.7 % for intermediate-bound protein) that were not used during the molecular replacement search.

The refinements were performed with *REFMAC5* Murshudov et al., 2011 and *BUSTER* (https://www.globalphasing.com) [8], with non-crystallographic symmetry (NCS) restrains for the apo and the pyruvate bond structures, and the models were manually corrected by using *COOT* [9]. All the structural figures were prepared with *PyMol* (The PyMOL Molecular Graphics System, Version 2.5.0 Schrödinger, LLC).

The atomic coordinates and the structure factors have been deposited in the Protein Data Bank (www.pdb.org) with accession numbers 9frt (apo protein), 9fxr (pyruvate-bound protein), and 9ftk (intermediate-bound protein) (Table 1).

Table 1
X-ray data-collection and refinement statistics.

Crystal	apo	pyruvate	intermediate
ligand	PO_4^{3-}	pyruvate	(R)-4-hydroxy-4-(2-hydroxyphenyl)-2-oxobutanoate
Crystallization conditions	$NH_4H_2PO_4$, 0.4 M	Na/KH_2PO_4, 0.8 M, HEPES pH 7.5	$NH_4H_2PO_4$, 0.4 M
Soaking/co-crystallization	–	pyruvate (10 mM)	pyruvate (2.5 mM) & salicylaldehyde (2.5 mM)
Beam line & wavelength (Å)	ESRF ID14-1 0.9334	ESRF ID23-1 0.97925	ESRF ID23-1 1.0718
Space group	C2	C2	I2
Unit-cell parameters (Å, °)	a = 199.7; b = 199.9; c = 144.1; β = 133.8	a = 200.2; b = 200.4; c = 144.5; β = 133.8	a = 144.5; b = 199.7; c = 144.5; β = 92.6
Resolution (Å)	36.04–1.96 (2.06–1.96)[a]	117.2–2.30 (2.34–2.30)[b]	46.7–1.76 (1.85–1.76)[c]
Unique reflections	277,447 (40,163)[a]	165,206 (8709)[b]	366,454 (53,349)[c]
Completeness (%)	95.6 (94.7)	91.4 (96.8)	90.5 (90.3)
Redundancy	2.0 (1.9)	2.4 (2.3)	2.0 (2.0)
Rmeas[a] (%)	13.4 (21.8)	25.1 (155.0)	10.7 (61.0)
CC(1/2) (%)	93.3 (89.7)	96.7 (37.1)	99.4 (81.9)
Average I/σ (I)	5.1 (3.4)	4.1 (1.3)	6.2 (1.4)
R factor[b]/Rfree[c] (%)	13.9/16.8	20.0/22.6	17.7/21.5
r.m.s. bonds (Å)	0.011	0.0076	0.0096
r.m.s. angles (°)	0.87	0.57	0.73
Ramachandran favored/ additionally allowed regions (%)	98/2	98/2	98/2
PDB-ID	9frt	9fxr	9ftk

Values in parentheses are for the highest resolution shell: [a](2.06–1.96), [b](2.34–2.30), [c](1.85–1.76).

[a] $R_{meas} = (\Sigma\ (n/(n-1)\ \Sigma\ |I - (I)|)/\Sigma\ I$ x 100, where I is intensity of a reflection and (I) is its average intensity.

[b] $R_{factor} = \Sigma\ |F_o - F_c|/\Sigma\ |F_o|$ x 100.

[c] R_{free} is calculated on 5 % randomly selected reflections, for cross-validation.

3. Results

3.1. Crystal structure of the apo protein

During the refinement of the apo crystal (2 tetramers in the crystal asymmetric unit (a.u.)), despite good agreement between the refined model and the electron density, we could not reduce the R/Rfree values

below 24.5/28.7, suggesting the presence of crystal twinning (twinning fraction calculated from H-test/L-test were 0.28/0.05 (program *scala* [4]). Further refinements using *REFMAC5* [10] which accounted for the twinning, reduced the R/Rfree values to 13.9/16.8.

In the final refined apo structure, the protein active site is occupied by a phosphate ion that interacts with the side chains of the catalytic amino acids Lys183 (distance 2.7 Å) and Tyr155 (2.6 Å), as well as with the main chain nitrogen of Thr65 (3.1 Å) and Phe66 (3.0 Å) in the conserved GXXGE motif (64-GTFGE-68 in our protein) (Fig. 1A). Notably, among the other residues in the active site, the side chain of Ile22 exhibits two distinct conformations, suggesting its possible role in substrate orientation, potentially influencing the precise positioning of the carboxylic group of pyruvate. A conserved water molecule (W1), present in all the 8 molecules in the a.u. (and in the structure of apo NahE (pdb-id 6dao)), establishes H-bonds with the phosphate ion (2.9 Å) and with the main chain nitrogen of Gly64 (2.9 Å) and Gly67 (2.8 Å) in the conserved GXXGE motif. The amine group of the catalytic Lys183 points toward the exterior of the protein, specifically toward Phe274 (Fig. 1A), forming a H-bond with another conserved water molecule (W2, 3.1 Å), further stabilized by the interaction with the main chain carbonyl of Lys183 (2.7 Å). W2 (not observed in the structures of *P. putida* aldolase NahE) may act as a hydrogen acceptor during the deprotonation of Lys in the initial phase of the Schiff base formation reaction (Scheme 1A). Additionally, near the protein's active site, a glycerol molecule is present, interacting with the phenolic ring of Tyr184 and the main chains of Leu185 and Gly186 (Fig. 1A and Fig. S1). The consistent presence of glycerol across all analyzed crystals shows the presence of an internal cavity, suggesting the possibility that this location might serve as a transient docking site for substrate or product diffusion to and from the enzyme's active site, whose access could be regulated by the side chain of Leu185.

Comparison of our apo structure with that of the homologous protein NahE from *P. putida* (pdb-id 8do5; [7]) bound to the intermediate compound (r.m.s.d: 0.364 Å on 322 aa.), revealed notable differences in a helix-loop-helix motif involving amino acids 268–277, located between alpha helices α(252–265) and α(274–279). This region of the protein, particularly the side chains of Leu268, Phe269, Phe274, and Phe277 may function as a hydrophobic lid to protect the active site from the solvent, as described by LeVieux et al. [11]. In our apo structure, the lid adopts a more open conformation, likely facilitating substrate(s) entry. Conversely in the NahE intermediate-bound structure the lid is more closed, likely serving to protect the intermediate Schiff base adduct from premature hydrolysis. Interestingly, in another apo structure of NahE from *P. putida* (pdb-id 6dao; [11]) the hydrophobic lid is closed in one of the two molecules in the crystal a.u. (chain A) and open in the other (chain B), indicating the intrinsic plasticity of this protein region. Notably, the open lid in chain B is associated with an open conformation of Leu185, the aforementioned gate to the active site from the Tyr184 docking site.

3.2. Crystal structure of the pyruvate-bound protein

The crystal structure of the protein bound to pyruvate provides additional insights into the catalytic mechanism. Indeed, after the deprotonation of the Lys183 in the active site (Scheme 1A), likely facilitated by the water molecule W2 (Fig. 1A), a covalent bond is formed between Lys183 and pyruvate, as expected in the initial phase of the aldol condensation reaction (Scheme 1A-D). Pyruvate is a small molecule that can easily diffuse toward the active site using multiple pathways. In our crystal structure, obtained by soaking the crystal for 1 min with 10 mM pyruvate, we observe a pyruvate molecule covalently bound to Lys183. In this structure, the C–N bond of the Lys183 side chain flips by ~130° toward the interior of the protein (i.e. toward Phe66 and Ile22) compared to the apo structure (Fig. 2A). This reorientation likely protects the new covalent adduct from hydrolysis. Interestingly, only one of the two conformations observed for Ile22 in the apo protein can be maintained in the Schiff base adduct to allow the placement of the carboxylic group of pyruvate (Fig. 1B). The water molecule W2, after fulfilling its putative function in deprotonating Lys183 (Scheme 1A), disappears from the active site, whereas W1 is still present and in contact with the carboxylic group of pyruvate (2.4 Å, Fig. 1B). The presence on an additional pyruvate molecule in the active site (each pyruvate was modelled with 50 % occupancy), closely positioned but not covalently bound to Lys183 (Fig. 1B and. 2A and Fig. S2), suggests a pre-reactive state conformation assumed shortly before the formation of the covalent adduct (Scheme 1B). In this configuration, the distance between the carbonyl group of pyruvate and the hydroxyl moiety of Tyr155 (~2.5 Å) is appropriate for the hydrogen transfer at the beginning of the reaction (Scheme 1B), with the pyruvate carbon atom at ~3.7 Å from the amine group of Lys183 in its apo conformation (Fig. 2A).

3.3. Crystal structure of the intermediate bound protein

The crystal structure featuring the Schiff base covalent adduct of the intermediate compound was obtained by co-crystallizing the protein in the presence of pyruvate and salicylaldehyde. For the activation of the nucleophilic carbon of the modified Lys183, another base is required (Scheme 1D). This role can be fulfilled either by a water molecule (assisted by Asn157 and Asn281) or by the side chain of Tyr155 (at 3.3 Å

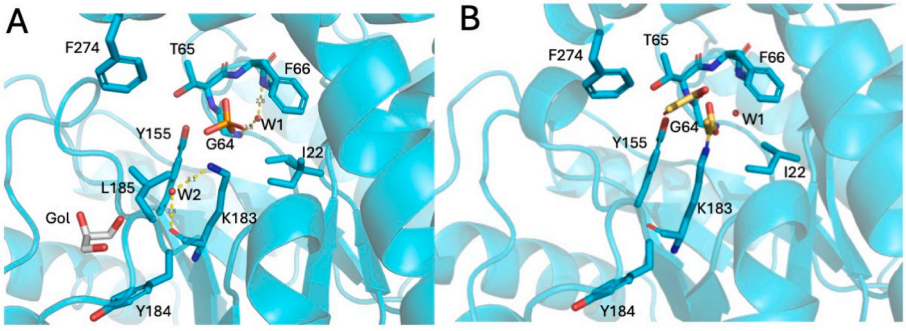

Fig. 1. A) Apo structure with a phosphate ion in the active site. Two conserved water molecules are shown: W1 (interacting with the G(64)TFGE motif) and W2, which may be involved in the deprotonation of the catalytic Lys. A conserved glycerol molecule (Gol, white carbon atoms), sitting onto the side chain of Tyr184 suggests a temporary docking site for substrate/product diffusion to/from the active site. The double conformation of Ile22 and the side chain of one the lid amino acid F274 are also shown. **B)** Pyruvate-bound structure. The active site hosts two pyruvate molecules, each modelled with 50 % occupancy (depicted with yellow carbon atoms): upper-left/unbound, and lower-right/covalently bound to Lys183. The conserved water molecule W1, the single conformation of Ile22, and selected amino acids of the GXXGE motif are also shown. (For interpretation of the references to color in this figure legend, the reader is referred to the Web version of this article.)

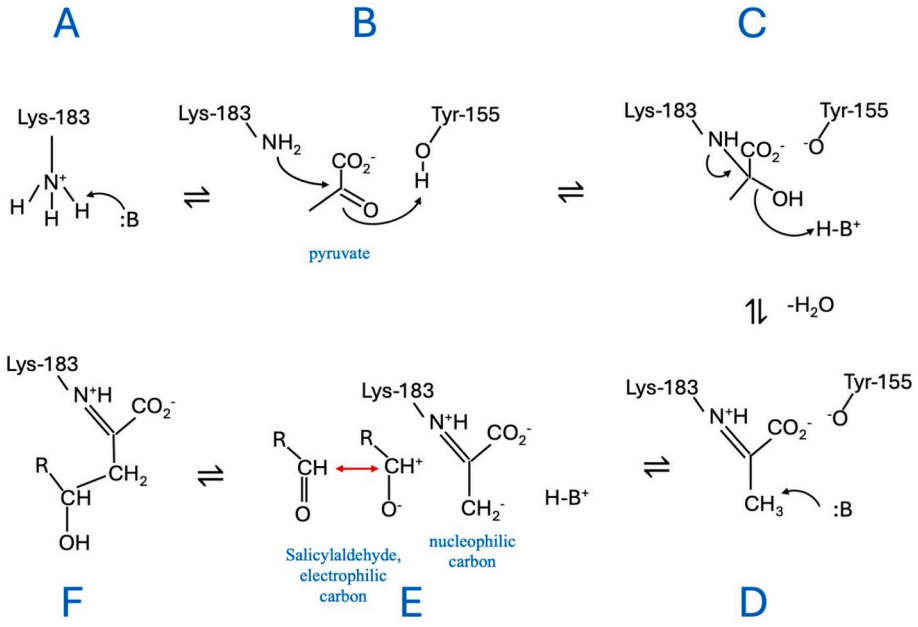

Scheme 1. The Aldol condensation reaction, adapted from Ref. [7].

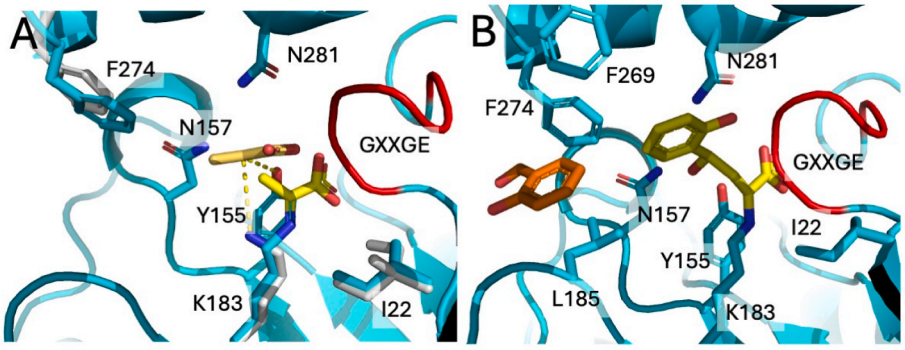

Fig. 2. A) Superposition of pyruvate-bound structure (cyan carbon atoms) and apo structure (gray carbon atoms for residues F274, K183 and I22). The two conformations of pyruvate in the active site, each modelled with 50 % occupancy, are shown (yellow carbon atoms). The different orientation of the active Lys183, the open/closed positions of Phe274 - one of the lid amino acid - and the double/single conformations of Ile22 in either the apo (gray carbon atoms) or pyruvate-bound form (cyan carbon atoms) are shown. The conserved GXXGE motif is colored in red. **B)** Intermediate-bound structure: cyan carbon atoms for protein and yellow carbon atom for the intermediate compound. An additional salicylaldehyde molecule present in the crystal is shown with orange carbon atoms. (For interpretation of the references to color in this figure legend, the reader is referred to the Web version of this article.)

distance in the pyruvate-bound structure).

In the intermediate-bound structure, the hydroxy group of (R)-4-hydroxy-4-(2-hydroxyphenyl)-2-oxobutanoate forms hydrogen bonds with the side chain of Tyr155 (3.0 Å) and the amide of Asn157 (3.3 Å) (Fig. 2B). The hydroxyl group of the salicylaldehyde portion forms hydrogen bonds with the side chains of Glu285 (2.6 Å) and Asn281 (3.4 Å), while its phenolic ring is in close contact with the side chains of Phe269, Phe274, and Phe277 and Trp224.

Notably, another salicylaldehyde molecule is positioned in proximity of the phenolic ring of the covalently bound intermediate (~3.5 Å), stabilized by Phe274 and Phe269 (belonging to the mentioned hydrophobic lid) and by Leu185 (Fig. 2B). This evidence suggests that the salicylaldehyde entry may occur through the hydrophobic lid. Conversely, it is plausible that pyruvate can accesse the active site from the opposite side, specifically through the conserved GXXGE motif (Fig. 2, highlighted in red). This spatial arrangement supports a model where, at steady state, the substrates follow two distinct pathways converging to the active site, optimizing the conditions for the aldol condensation reaction. The narrow path through the GXXGE motif, which is intrinsically flexible due to the presence of the two glycine residues, is assumed to be accessible mainly to small compounds and may restrict access to larger molecules. Besides, this path could also be allosterically regulated by the neighboring Trp128 from another aldolase molecule in the tetramer (Fig. S3).

4. Discussion

Aldolases, due to their role in carbon-carbon bond formation, have been extensively studied for their potential in efficiently synthesizing a wide range of organic chemicals [12,13].

This study offers significant insights into the molecular and catalytic mechanisms of aldolase enzymes, with a focus on the structural analysis of tHBP-HA from *P. fluorescens* N3. tHBP-HA is a class I aldolase that relies strictly on pyruvate to catalyze the reversible transformation of *trans-o*-hydroxybenzylidenepyruvate (t-HBP) into pyruvate and salicylaldehyde.

Previous work characterized the aldol condensation activity of tHBP-HA using pyruvate as a substrate with either salicylaldehyde or

benzaldehyde [2]. The measured K_m values indicated that tHBP-HA shows a slightly higher affinity for salicylaldehyde (3.6 mM) compared to benzaldehyde (9.0 mM). This preference is likely due to favorable interactions between the hydroxyl group of salicylaldehyde and the side chains of Glu285 and Asn281, a preference also reflected in the Vmax values (17.2/35.5 μmol mg^{-1} min^{-1}, respectively). Further investigations have explored the enzyme catalytic activity using other aldehydes with different electron demand, leading to the synthesis of α-β-unsaturated oxoacids and furan derivatives [14]. In comparison, other aldolase enzymes, such as the recombinant NahE from *P. putida,* have been shown to catalyze stereoselective nitro-Michael reaction to produce β-aryl-γ-nitrobutyric acids from a variety of aldehydes [15].

Our structural studies provide a detailed view of the enzyme active site and the dynamic nature of its catalytic mechanism. By analyzing the apo and pyruvate-bound structures, alongside comparisons with homologous enzymes, we gain insights into substrate entry, intermediate stabilization, and potential regulation of enzymatic activity through conformational flexibility.

Notably, our three-state crystallographic snapshots of tHBP-HA reveal minimal conformational changes in the active site during the various phases of aldol condensation. This observation suggests that the enzyme chemistry is highly optimized, requiring minimal movements for catalysis, with most chemical changes occurring at the level of electron and hydrogen distribution within the involved groups.

At the onset of aldol condensation, the lid adopts an open conformation, exposing the active site to the pyruvate substrate and facilitating the formation of the Schiff base. This process is aided by the conserved water molecule W2, which plays a crucial role in the deprotonation of the catalytic lysine, highlighting a critical step in the enzymatic process. As the reaction proceeds, the lid closes, likely preventing the release of the intermediate compound, and the covalently modified enzyme becomes poised for the second reaction between the activated nucleophilic enamine (potentially facilitated by Tyr155 acting as a base) and the electrophilic salicylaldehyde. Given that the lid is already closed after the covalent linkage with pyruvate, salicylaldehyde may access the active site through the Tyr184-Leu185 gate, observed as a glycerol docking site. At steady state the two substrates could diffuse through two different pathways modulated by the oscillation of both the lid and the GXXGE motif. Moreover, the observation that the narrow path through the GXXGE motif might be allosterically regulated by Trp128 from another aldolase molecule in the tetramer suggests the potential for a cooperative behavior within the enzyme quaternary structure, offering a new perspective on how enzyme activity could be influenced by protein-protein interactions.

Overall, these findings contribute to a deeper understanding of the molecular and structural mechanisms governing tHBP-HA function and hold potential for future efforts to manipulate its activity for biotechnological applications.

CRediT authorship contribution statement

Silvia Ferrara: Conceptualization, Data curation, Formal analysis, Investigation, Methodology, Writing – original draft, Writing – review & editing. **Bianca Braggiotti:** Formal analysis. **Eloise Mastrangelo:** Validation, Writing – original draft. **Patrizia Di Gennaro:** Conceptualization, Methodology. **Giovanni Bertoni:** Conceptualization, Methodology. **Mario Milani:** Conceptualization, Data curation, Formal analysis, Investigation, Methodology, Supervision, Validation, Writing – original draft, Writing – review & editing.

Declaration of competing interest

The authors declare the following financial interests/personal relationships which may be considered as potential competing interests: Mario Milani reports administrative support and equipment, drugs, or supplies were provided by European Union. If there are other authors, they declare that they have no known competing financial interests or personal relationships that could have appeared to influence the work reported in this paper.

Acknowledgments

We thank the beam line scientists of the ESRF beam lines id14-1 and id23-1 for support during data collections. We thank the European Union - Next Generation EU - PNRR, MUR code IR0000011, CUP B51E22000150006, project 'EBRAINS-Italy' for the use of the X-ray structure solution platform.

Appendix A. Supplementary data

Supplementary data to this article can be found online at https://doi.org/10.1016/j.bbrc.2024.151281.

References

[1] P. Di Gennaro, E. Galli, G. Albini, F. Pelizzoni, G. Sello, G. Bestetti, Production of substituted naphthalene dihydrodiols by engineered Escherichia coli containing the cloned naphthalene 1,2-dioxygenase gene from Pseudomonas fluorescens N3, Res. Microbiol. 148 (4) (1997) 355–364, https://doi.org/10.1016/S0923-2508(97)81591-4.

[2] S. Ferrara, E. Mapelli, G. Sello, P. Di Gennaro, Characterization of the aldol condensation activity of the trans-o-hydroxybenzylidenepyruvate hydratase-aldolase (tHBP-HA) cloned from Pseudomonas fluorescens N3, Biochim. Biophys. Acta 1814 (5) (2011) 622–629, https://doi.org/10.1016/J.BBAPAP.2011.03.013.

[3] T.G.G. Battye, L. Kontogiannis, O. Johnson, H.R. Powell, A.G.W. Leslie, iMOSFLM: a new graphical interface for diffraction-image processing with MOSFLM, Acta Crystallographica Section D: Biological Crystallography 67 (Pt 4) (2011) 271, https://doi.org/10.1107/S0907444910048675.

[4] P. Evans, Scaling and assessment of data quality, Acta Crystallographica. Section D, Biological Crystallography 62 (Pt 1) (2006) 72–82, https://doi.org/10.1107/S0907444905036693.

[5] C. Vonrhein, C. Flensburg, P. Keller, A. Sharff, O. Smart, W. Paciorek, T. Womack, G. Bricogne, Data processing and analysis with the autoPROC toolbox, Urn:Issn: 0907-4449 67 (4) (2011) 293–302, https://doi.org/10.1107/S0907444911007773.

[6] A. Vagin, A. Teplyakov, MOLREP: an automated program for molecular replacement, Urn:Issn:0021-8898 30 (6) (1997) 1022–1025, https://doi.org/10.1107/S0021889897006766.

[7] E.B. Lancaster, W.H. Johnson, J.A. LeVieux, H.A. Hardtke, Y.J. Zhang, C. P. Whitman, A mutagenic analysis of NahE, a hydratase-aldolase in the naphthalene degradative pathway, Arch. Biochem. Biophys. 733 (2023) 109471, https://doi.org/10.1016/J.ABB.2022.109471.

[8] E. Blanc, P. Roversi, C. Vonrhein, C. Flensburg, S.M. Lea, G. Bricogne, Refinement of severely incomplete structures with maximum likelihood in BUSTER-TNT, Acta Crystallographica. Section D, Biological Crystallography 60 (Pt 12 Pt 1) (2004) 2210–2221, https://doi.org/10.1107/S0907444904016427.

[9] P. Emsley, B. Lohkamp, W.G. Scott, K. Cowtan, Features and development of coot, Acta Crystallographica. Section D, Biological Crystallography 66 (Pt 4) (2010) 486–501, https://doi.org/10.1107/S0907444910007493.

[10] G.N. Murshudov, P. Skubák, A.A. Lebedev, N.S. Pannu, R.A. Steiner, R.A. Nicholls, M.D. Winn, F. Long, A.A. Vagin, REFMAC5 for the refinement of macromolecular crystal structures, Acta Crystallographica. Section D, Biological Crystallography 67 (Pt 4) (2011) 355–367, https://doi.org/10.1107/S0907444911001314.

[11] J.A. LeVieux, B. Medellin, W.H. Johnson, K. Erwin, W. Li, I.A. Johnson, Y.J. Zhang, C.P. Whitman, Structural characterization of the hydratase-aldolases, NahE and PhdJ: implications for the specificity, catalysis, and N-acetylneuraminate lyase subgroup of the aldolase superfamily, Biochemistry 57 (25) (2018) 3524–3536, https://doi.org/10.1021/ACS.BIOCHEM.8B00532/ASSET/IMAGES/LARGE/BI-2018-00532R_0010.JPEG.

[12] S.H. Lee, S.J. Yeom, S.E. Kim, D.K. Oh, Development of aldolase-based catalysts for the synthesis of organic chemicals, Trends Biotechnol. 40 (3) (2022) 306–319, https://doi.org/10.1016/J.TIBTECH.2021.08.001.

[13] K. Fesko, M. Gruber-Khadjawi, Biocatalytic methods for C-C bond formation, ChemCatChem 5 (6) (2013) 1248–1272, https://doi.org/10.1002/CCTC.201200709.

[14] G. Sello, P. Di Gennaro, Aldol reactions of the trans-o-hydroxybenzylidenepyruvate hydratase-aldolase (tHBP-HA) from Pseudomonas fluorescens N3, Appl. Biochem. Biotechnol. 170 (7) (2013) 1702–1712, https://doi.org/10.1007/S12010-013-0302-3.

[15] D.J. Fansher, D.R.J. Palmer, D.J. Fansher, D.R.J. Palmer, A type 1 aldolase, NahE, catalyzes a stereoselective nitro-michael reaction: synthesis of β-Aryl-γ-nitrobutyric acids, Angew. Chem. Int. Ed. 62 (6) (2023) e202214539, https://doi.org/10.1002/ANIE.202214539.